Research Article

C. Raveendiran, P. Prabukanthan*, J. Madhavan, P. A. Vivekanand*, Natarajan Arumugam, Abdulrahman I. Almansour, Raju Suresh Kumar, Shatha Ibrahim Alaqeel, and Karthikeyan Perumal

Synthetic pathway of 2-fluoro-N,N-diphenylbenzamide with opto-electrical properties: NMR, FT-IR, UV-Vis spectroscopic, and DFT computational studies of the first-order nonlinear optical organic single crystal

https://doi.org/10.1515/gps-2022-0097 received April 30, 2022; accepted December 13, 2022

Abstract: 2-Fluoro-*N*,*N*-diphenylbenzamide (2FNNDPBA), a natural nonlinear optical (NLO) single crystal, was incorporated from diphenylamine utilizing 2-fluoro benzoyl chloride as a side chain. The single crystals were successfully developed by a slothful evaporation arrangement approach utilizing ethyl acetate as a dissolvable solvent at room temperature. The synthesized compound fragmented ion peak (m/z=291) was affirmed by gas-chromatographic mass spectrometry investigation. The unit cell dimensions were assessed using single-crystal X-ray diffraction analysis, which reveals that the crystals possess the orthorhombic system with space group *Pbca*. The existence of proton and carbon in a compound was affirmed by 1 H and 13 C nuclear magnetic resonance. The functional

groups therein of 2FNNDPBA have been identified from FT-IR and FT-Raman studies and amide carbonyl stretching frequency peak appeared at 1,662 cm⁻¹. The lower cut-off wavelength of 2FNNDPBA is found to be 240 nm and the experimental and theoretical optical band gap was calculated as 3.21 and 3.1083 eV. The UV-Visible spectrum of 2FNNDPBA shows two high-flying peaks at 240 and 273 nm. Major weight losses were observed between 160°C and 275°C for the designated compound. The thermal property for 2FNNDPBA was estimated by thermogravimetric analysis/differential thermal analysis investigation, which shows immense thermal strength up to 171°C. Density functional theory method with Gaussian 09 software for theoretical investigations of 2FNNDPBA for Mulliken charge analysis, highest occupied molecular orbital-lowest-lying unoccupied molecular orbital, and molecular electrostatic potential properties has been analyzed. The SHG productivity was proved by Kurtz-Perry powder strategy and has an efficiency 2.22 times that of standard potassium dihydrogen phosphate. The laser damage threshold of 2FNNDPBA crystals was discovered to be 1.18 GW·cm⁻². The hyperpolarizability simulations further show that the current material has an excellent NLO activity tendency. The melting point of the developed crystal is 158°C.

Keywords: X-ray diffraction, optical spectrum, DFT, benzamide, crystal growth

* Corresponding author: P. Prabukanthan, Materials Chemistry Lab,

Department of Chemistry, Muthurangam Government Arts College,

J. Madhavan: Solar Energy Lab, Department of Chemistry, Thiruvalluvar University, Vellore, 632115, India

Natarajan Arumugam, Abdulrahman I. Almansour, Raju Suresh Kumar: Department of Chemistry, College of Science, King Saud University, P.O. Box 2455, Riyadh 11451, Saudi Arabia Shatha Ibrahim Alaqeel: Department of Chemistry, College of Science, King Saud University (034), Riyadh 11495, Saudi Arabia Karthikeyan Perumal: Department of Chemistry and Biochemistry, The Ohio State University, 151W. Woodruff Ave, Columbus, OH 43210, USA

1 Introduction

Fluorine substituted new molecules assume a critical part in crystals designing for investigating its plausible towards mechanical applications [1]. In the hunt for innovative significant materials, specialists are drawn to and

Vellore 632002, India, e-mail: pprabukanthan76@hotmail.com
* Corresponding author: P. A. Vivekanand, Centre for Catalysis
Research & Department of Chemistry, Saveetha Engineering
College, Chennai 602105, India, e-mail: pavivek@rediffmail.com
C. Raveendiran: Materials Chemistry Lab, Department of Chemistry,
Muthurangam Government Arts College, Vellore 632002, India

deal with organic molecules because of the existence of delocalized π -electronic constructions. The π -conjugated framework in organic molecules existing electron benefactor and acceptor bunches makes the material show a high second harmonic proficiency response [2,3]. In addition, the nonlinear reaction of the organic π -conjugated framework relies upon the crystallinity of the molecule [4]. The point is to discover and foster nonlinear optical (NLO) materials [5–7] outfitting huge nonlinearities and simultaneously satisfying every one of the innovative requirements for applications, for example, wide straightforwardness range, quick reaction, and interfacing with different materials [8]. Density functional theory (DFT) approaches have become accepted in recent years due to their high precision in reproducing investigational values of molecular geometry, vibrational frequencies, dipole moment, and atomic charges, among other things [9–16].

In this point of view, the present work is designed to synthesis 2-fluoro-N,N-diphenylbenzamide (2FNNDPBA) and to develop as single crystals. 2FNNDPBA is an intriguing compound, aryl tertiary amide, whose synthetic construction is profoundly delocalized π -electron framework in which fluorine is substituted in the benzene ring. The developed single crystals will be described for their NLO applications. Their trademark studies, for example, primary, otherworldly, optical, and thermal are to be completed and the outcomes are accounted for [17]. Experiments and theoretical investigations will be conducted to afford a complete depiction of the molecular structure, first-order hyperpolarizability, Mulliken atomic charges, highest occupied molecular orbital (HOMO)-lowest-lying unoccupied molecular orbital (LUMO) analysis, and molecular electrostatic potential (MEP), among other things.

2 Experimental and computational details

2.1 Materials

N,N-Diphenylamine (99%; Sigma-Aldrich), 2-fluorobenzoylchloride (99%; Sigma-Aldrich), dry acetonitrile (99.8%; Merck), and triethylamine (Extra pure, SRL) were procured from commercial sources and used as such.

2.2 Synthesis of 2FNNDPBA compound

The combination of 2FNNDPBA was effectively done by the synthetic response between cheaply accessible N,N-diphenylamine and 2-fluorobenzoylchloride bought from Sigma-Aldrich. An improved method was utilized for the benzoylation of amine. Diphenylamine (1 mmol, 0.5 g) liquefies in dry acetonitrile (10 vol%) with the growth of triethylamine (1.2 mmol, 0.36 g) used as a base. The reaction mixture was cooled to 0-5°C and to this arrangement 2-fluorobenzylchloride (1.05 mmol, 0.49 g) was added drop by drop pending the adding up was finished. The reaction mixture was agitated for 60 min at 60°C mode. The reaction progress was observed in thin layer chromatography (TLC), once reaction was completed, the core mass was cooled to room temperature and filled with ice water under Verger's agitation. The appeared crude solid filtered through Whatman filter paper was washed with de-ionized water and then dried at room temperature. Dried crude material dissolved in ethyl acetate for crystallization (yield: 88%). The molecular ion peak at 291 was affirmed by gas chromatographic mass spectrometry (GC-MS) (Figure 1). The preparation of 2FNNDPBA is represented in Scheme 1.

2.3 Crystal growth

The soaked arrangement of 2FNNDPBA with ethyl acetate as a dissolvable solvent was blended ceaselessly for 30 min to make it homogeneous at room temperature. The dissolvability was assessed at room temperature in ethyl acetate, ethanol, methanol, acetone, and DMSO. Among the four solvents utilized, DMSO was discovered to be the best dissolvable for the bulk growth of 2FNNDPBA; however, the crystal growth did not seem to be steady. Consequently, the soaked collection was arranged by utilizing ethyl acetate and separated by means of Whatman filter paper (grade No. 1). The measuring utensil containing the arrangement was then ideally shut and reserved at room temperature for moderate dissipation. After 2 days, optically transparent single crystals were reaped with the components of $6 \, \text{mm} \times 3 \, \text{mm} \times 2 \, \text{mm}$. The seemed crystals are more stable, colorless, transparent, and non-hygroscopic at room temperature as shown in Figure 2. The melting point of the developed crystals was exposed to be 158°C.

2.4 Computational details

The molecular structure of 2FNNDPBA in the ground state (in vacuo) was optimized using the density functional theory DFT/B3LYP technique with the 6-311++G(d,p) [18] basis. For 2FNNDPBA, the entire computation was done

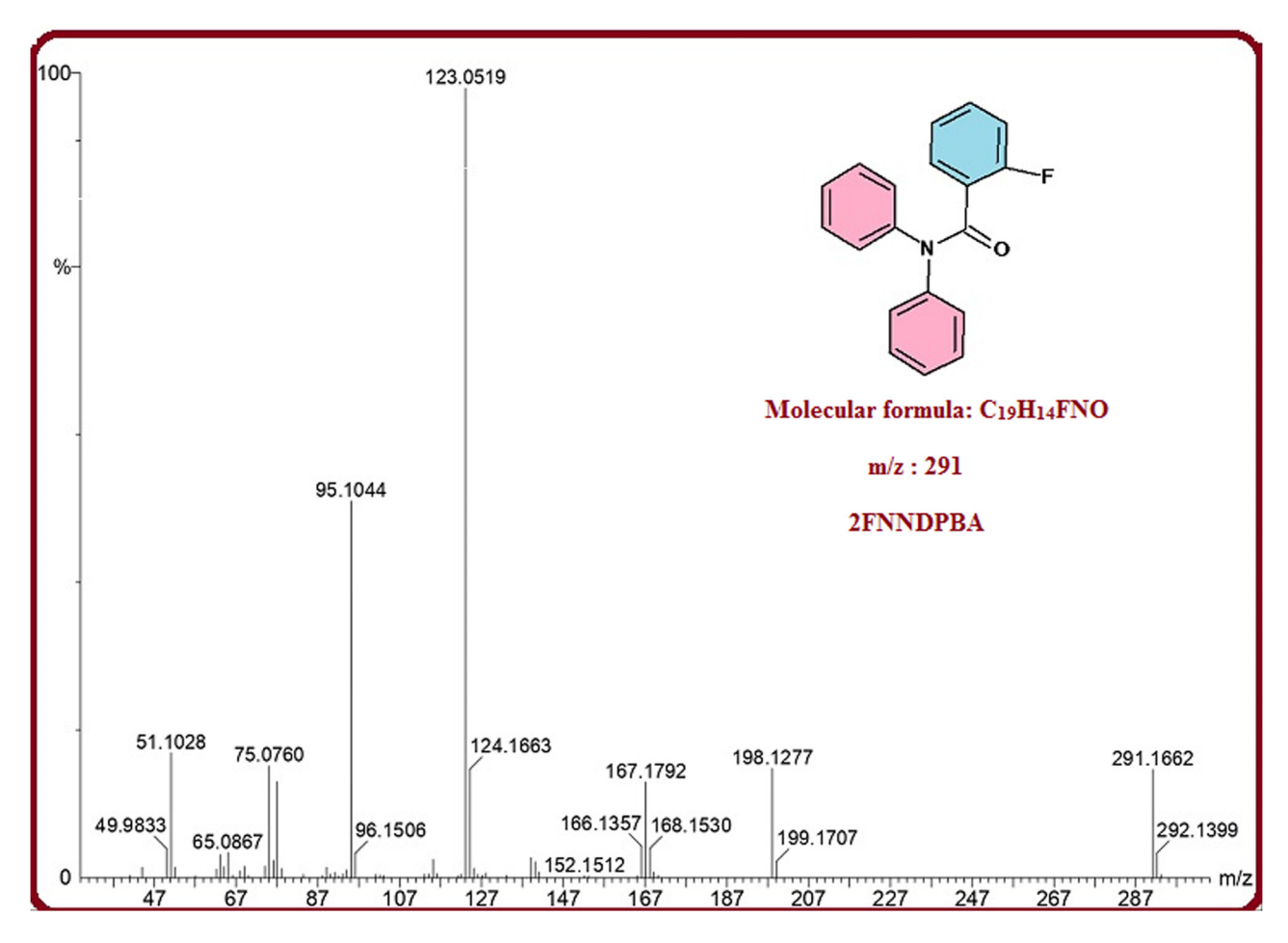


Figure 1: GC-MS molecular ion peak diagram of 2FNNDPBA.

without defining and symmetry, utilizing Gauss view molecular visualization application [19] and Gaussian 09 program package [20] for modeling the compound's first guess and was first acquired from the X-ray measurements. The harmonic vibrational frequencies were estimated at the B3LYP/6-311++G(d,p) level of hypothesis for

the optimized structure. Based on the finite-field technique [21], the first-order hyperpolarizability (β) of 2FNNDPBA was computed using the B3LYP/6-311++G(d,p) foundation set. Furthermore, the same degree of theory was applied to HOMO–LUMO, Mulliken charges, MEP, and van der Waals interaction features.

Scheme 1: Synthesis of 2FNNDPBA: (1) N-phenylaniline, (2) 2-fluorobenzoyl chloride, and (3) 2FNNDPBA.

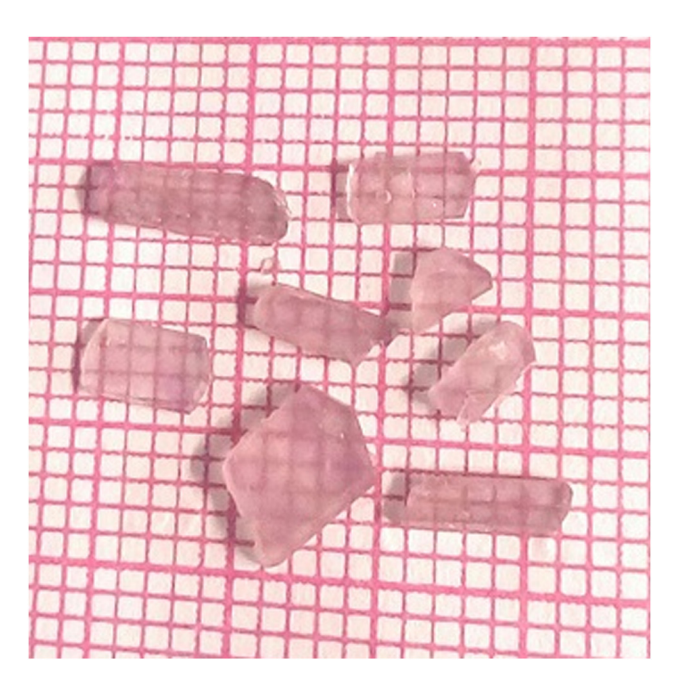


Figure 2: Grown single crystal image of 2FNNDPBA.

3 Results and discussion

3.1 Single crystal X-ray diffraction (XRD) analysis

Unit cell measurements and the crystal structure were resolved from a single crystal XRD record acquired with Bruker AXS Kappa APEX-II diffractometer outfitted with a graphite monochromatic MoK α ($\lambda = 0.7103 \text{ Å}$) radiation and CCD locator at a temperature of 25°C. The single crystal with a size of 0.250 mm \times 0.200 mm \times 0.200 mm was used for the XRD analysis. The SHELX software was utilized for data collection and as well for indexing the reflections. A total of 28,302 reflections was collected with 2θ range of 2.280–24.998° of which 2,619 reflections are measured as independent reflections with $I > 2\sigma(I)$. The structure was resolved by direct method utilizing the SHELXS97 [21] program and refined with SHELXL97 [22] by the full-lattice least-squares manner. The supreme fine-tuning was performed by full-matrix least-squares technique with anisotropic thermal boundaries for non-H-atoms on F^2 . The final refinement indices, R-values of $R_1 = 0.0538$ and $wR_2 = 0.1143$ and R indices (all data) $R_1 = 0.1492$ and w $R_2 = 0.1681$. Single crystal XRD investigation reveals that 2FNNDPBA belongs to orthorhombic crystal system with space group *Pbca*. The estimated lattice parameters are as follows: area = 17.381(6) A° , b = 9.559(3) Å, $c = 17.866(6) \text{ Å}, \beta = 90^{\circ}, \text{ and volume} = 2968.6(17) \text{ Å}^3. \text{ The}$ 2FNNDPBAcrystal data, investigational conditions, and

structural sophistication parameters are illustrated in Table 1. The crystallography software similar to PLATON [23], ORTEP [24], and MERCURY [25] was dilapidated for the geometric study and presentation of the consequences.

The ORTEP diagram with 40% probability level with its atom labeling method of 2FNNDPBA is given in Figure 3. The bond length and bond angle are listed in Table 2. The packing arrangement and hydrogen bonding of 2FNNDPBA molecules viewed along the "a" axis is shown in Figure 4. The packing arrangement shows that the C-H···O hydrogen bond produces more strengthening link between the two dimmers to form the stable crystal structure. The intermolecular and intra-molecular hydrogen bonding typically grip a hydrogen atom that is usually a hurdle to an electronegative atom such as oxygen and interacts using electrostatic forces with a different electronegative fluorine atom.

Table 1: Crystallographic data of 2FNNDPBA

Crystal data and structure refinement	2FNNDPBA
Identification code	2FNNDPBA
Empirical formula	$C_{19}H_{14}FNO$
Formula weight	291.31
Temperature	296(2) K
Wavelength	0.71073 Å
Crystal system	Orthorhombic
Space group	Pbca
Unit cell dimensions	$a = 17.381(6) \text{ Å}, \ \alpha = 90^{\circ}$
	$b = 9.559(3) \text{Å}, \beta = 90^{\circ}$
	$c = 17.866(6) \text{ Å}, \gamma = 90^{\circ}$
Volume	2968.6(17) Å ³
Z	8
Density (calculated)	1.304 mg⋅m ⁻³
Absorption coefficient	$0.089~{\rm mm}^{-1}$
F(000)	1216
Crystal size	0.250 mm $ imes$ 0.200 mm $ imes$
	0.200 mm
Theta range for data collection	from 2.280° to 24.998°
Index ranges	$-20 \le h \le 20$, $-11 \le k \le 11$, -21
	$\leq l \leq 20$
Reflections collected	28,302
Independent reflections	2,619 [$R(int) = 0.1348$]
Completeness to theta =	100%
24.998°	
Absorption correction	Semi-empirical from
	equivalents
Max. and min. transmission	0.7452 and 0.5631
Refinement method	Full-matrix least-squares on F^2
Data/restraints/parameters	2,619/0/200
Goodness of fit on F^2	1.000
Final R indices $[I > 2 \text{ sigma}(I)]$	$R_1 = 0.0538$, w $R_2 = 0.1143$
R indices (all data)	$R_1 = 0.1492$, w $R_2 = 0.1681$
Extinction coefficient	0.0037(7)
Largess diff. peak and hole	0.178 and −0.179 e·Å ^{−3}

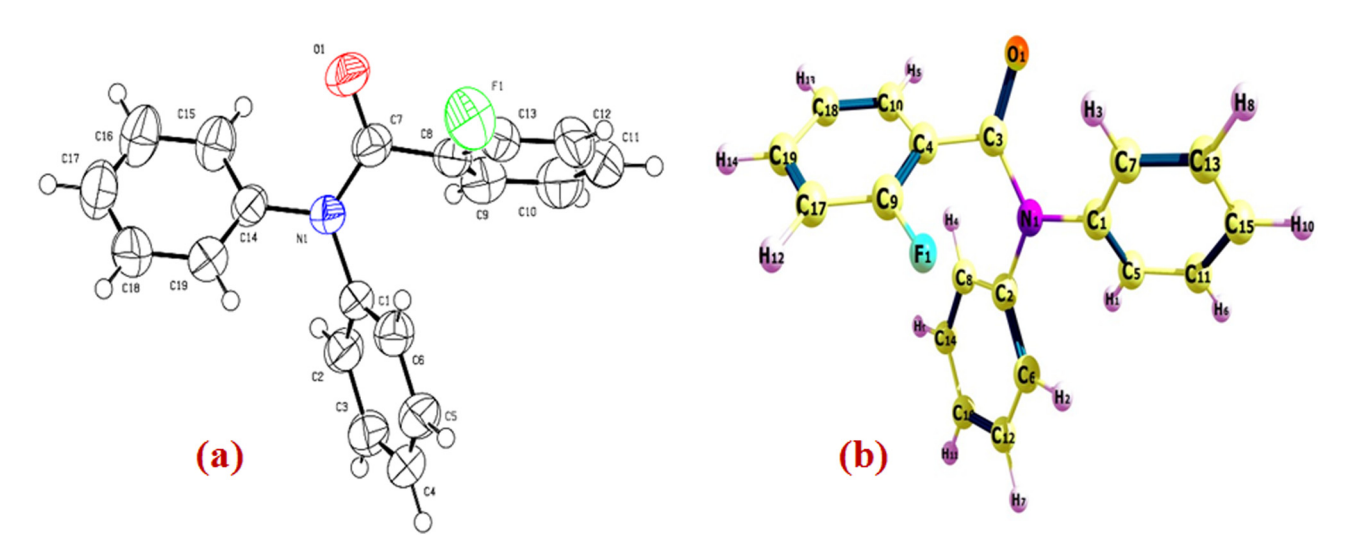


Figure 3: (a) ORTEP view of the molecule with displacement ellipsoids drawn at 40%. (b) The theoretical optimized geometric structure of $2FNNDPBA\ B3LYP/6-311++G(d,p)$ level.

The bond length and bond angles of hydrogen atoms of 2FNNDPBA are specified in Table 3.

The 2FNNDPBA single crystal deposited as CCDC no. 2082550 contains the accompanying crystallographic data for this article.

3.2 Optimized structure

The mathematical boundaries of 2FNNDPBA were determined at the B3LYP/6-311++G(d,p) level by the DFT strategy and recorded in Table 2, together with relating test esteems.

In Table 2, the greater part of the streamlined bond lengths are somewhat not the same as the exploratory outcomes, since the molecular states are diverse during the trial and hypothetical cycles. A few packing molecules are treated in the consolidated stage during exploratory (XRD) estimations, while one disengaged molecule is considered in the gas stage during the hypothetical (DFT) computation. There are 19 C–C bonds, 14 C–H bonds, 1 C–O bond, 3 C–N bonds, and 1 C–F bond in this molecule. The aromatic benzene rings of the 2FNNDPBA are rather uneven and the extent of bond distance for C–C is 1.218–1.508 Å (DFT) and 1.221–1.487 Å (XRD), that for

Table 2: Preferred structural parameters by XRD and DFT calculations of 2FNNDPBA

Parameters bond length (Å)	Experimental	B3LYP/6-311+ +G(d,p)	Parameters bond angle (°)	Experimental	B3LYP/6-311+ +G(d,p)
F(1)-C(13)	1.359(4)	1.356	C(2)-C(1)-C(6)	120.0(3)	119.74
C(1)-C(2)	1.373(5)	1.397	C(2)-C(1)-N(1)	118.8(3)	120.64
C(1)-C(6)	1.376(4)	1.397	C(6)-C(1)-N(1)	121.2(3)	119.60
C(1)-N(1)	1.442(4)	1.437	O(1)-C(7)-N(1)	122.1(3)	122.64
C(7)-O(1)	1.221(4)	1.218	O(1)-C(7)-C(8)	120.2(3)	119.42
C(7)-N(1)	1.371(4)	1.389	N(1)-C(7)-C(8)	117.6(3)	117.94
C(7)-C(8)	1.487(5)	1.508	C(13)-C(8)-C(9)	116.7(3)	117.34
C(14)-N(1)	1.429(4)	1.439	F(1)-C(13)-C(12)	118.2(4)	117.91
			F(1)-C(13)-C(8)	117.5(3)	119.38
			C(12)-C(13)-C(8)	124.3(4)	122.70
			C(15)-C(14)-C(19)	119.6(3)	119.79
			C(15)-C(14)-N(1)	120.6(3)	119.77
			C(19)-C(14)-N(1)	119.8(3)	120.39
			C(7)-N(1)-C(14)	120.4(3)	119.31
			C(7)-N(1)-C(1)	121.6(3)	122.74
			C(14)-N(1)-C(1)	117.3(3)	117.56

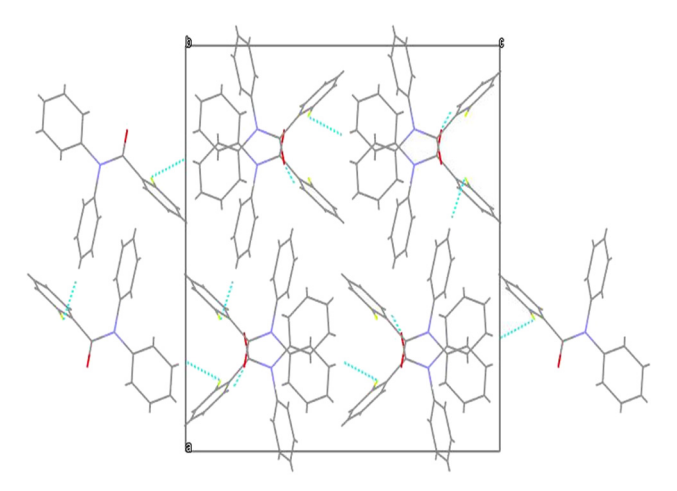


Figure 4: Packing arrangement and hydrogen bonding of 2FNNDPBA viewed along "a" axis.

carbonyl phenyl (C7–C8) ring is 1.508 Å (DFT) and 1.487 Å (XRD), for benzamide (O=C-NH-) (N1-C7) is 1.389 Å (DFT) and 1.371 Å (XRD), for fluorophenyl (F1–C13) ring is 1.356 Å (DFT) and 1.359 Å (XRD), respectively. The abovementioned bond lengths are very close to the experimental values.

3.3 UV-Vis-NIR spectral analysis

UV-Vis spectral technique is a primary technique to conclude the optical properties and transparency of a synthesized single crystal. The UV-Vis spectrum of 2FNNDPBA crystal was measured by means of Perkin-Elmer Lambda 35 spectrometer in the assortment of 200-800 nm. The measured UV-Vis absorption spectra of 2FNNDPBA crystal are displayed in Figure 5a. The spectrum of 2FNNDPBA shows two high-flying peaks at 240 and 273 nm. The basic necessity and advantage for a material having NLO properties are the nonexistence of absorption in the constituency 350-1,100 nm. The appeared two peaks correspond to $n-\pi^*$ and $\pi-\pi^*$ transition of the compound. The UV-Vis transmission spectrum (Figure 5b) is superior in visible and near infrared regions.

The optical (E_g) band gap of 2FNNDPBA single crystal was anticipated by using Tauc's plots $(\alpha h \nu)^2$ with energy (eV) and it is found to be 3.21 eV as shown in Figure 5c. Wide transparency of the sample can be used in optoelectronic applications.

3.4 FT-IR and Raman spectral study

The obtained FT-Raman and FT-IR spectra are shown in Figures 6 and 7, respectively. The observed spectrum reveals the of all the functional groups in the single crystal 2FNNDPBA. Shimadzu IRAffinity spectrometer was used to record the vibrational frequencies using KBr pellet technique in the wave number series from 400 to $4,000 \,\mathrm{cm}^{-1}$. The strong aromatic C-H stretching vibration appeared in IR at 3,060 cm⁻¹ and in Raman at 3,064 cm⁻¹. The tertiary amide carbonyl stretching vibrations were confirmed in IR at 1.662 cm⁻¹ and in Raman at $1,661 \,\mathrm{cm}^{-1}$. The region $1,650-1,430 \,\mathrm{cm}^{-1}$ corresponds to ring C-C stretching vibration in benzene derivatives and is usually selected to C=C stretching modes [26,27]. The FT-IR bands for C=C stretching vibrations occurred at 1,590 and 1,488 cm⁻¹ and occurred at 1,594 and 1492 cm⁻¹ in FT-Raman. The region at 1,626–1,294 cm⁻¹ is fixed for C–N stretching modes as per Chandran et al. [28,29]. The C-N stretching vibrations were observed at 1,346 cm⁻¹ in FT-IR and 1,347 cm⁻¹ in Raman. The aromatic fluoro compound (C-F) shows a strong vibrational frequency at 1,100–1,000 cm⁻¹. Fluorine substitution (C-F) in the title compound was also confirmed at 1,010 and 1,000 cm⁻¹ in FT-IR and Raman spectral data, respectively. Therefore, the FT-IR analysis was incorrigible on the whole molecular structure of the titled crystal. The recorded vibrational assignments for 2FNNDPBA single crystal are given in Table 4.

Table 3: Bond lengths and bond angles of hydrogen atoms of 2FNNDPBA (Å and °)

D-H A	d(D-H)	d(H A)	d(D A)	<(DHA)
C(15)-H(15) O(1) # (0)	0.930(0.004)	2.878(0.005)	2.587(0.003)	98.69(0.25)
C(4)-H(4) F(1) # (1)	0.930(0.004)	3.354(0.005)	2.547(0.002)	145.34(0.24)
C(5)-H(5) O(1) # (2)	0.930(0.004)	3.552(0.005)	2.980(0.003)	121.19(0.23)
C(4)-H(4) O(1) # (2)	0.930(0.004)	3.441(0.005)	2.760(0.003)	130.87 0.23)
C(9)-H(9)O(1) # (3)	0.930(0.004)	3.297(0.005)	2.411(0.003)	159.10(0.25)
C(18)-H(18) F(1) # (4)	0.930(0.004)	3.429(0.005)	2.612(0.002)	146.79(0.26)

Equivalent positions and symmetry transformations of the atoms: #(0) x, y, z; #(1) -x, +y - 1/2, -z + 1/2; #(2) x - 1/2, +y, -z + 1/2; # (3) -x + 1/2, +y - 1/2, +z; # (4) -x + 1/2, -y + 1, +z - 1/2.

1154 — C. Raveendiran et al. DE GRUYTER

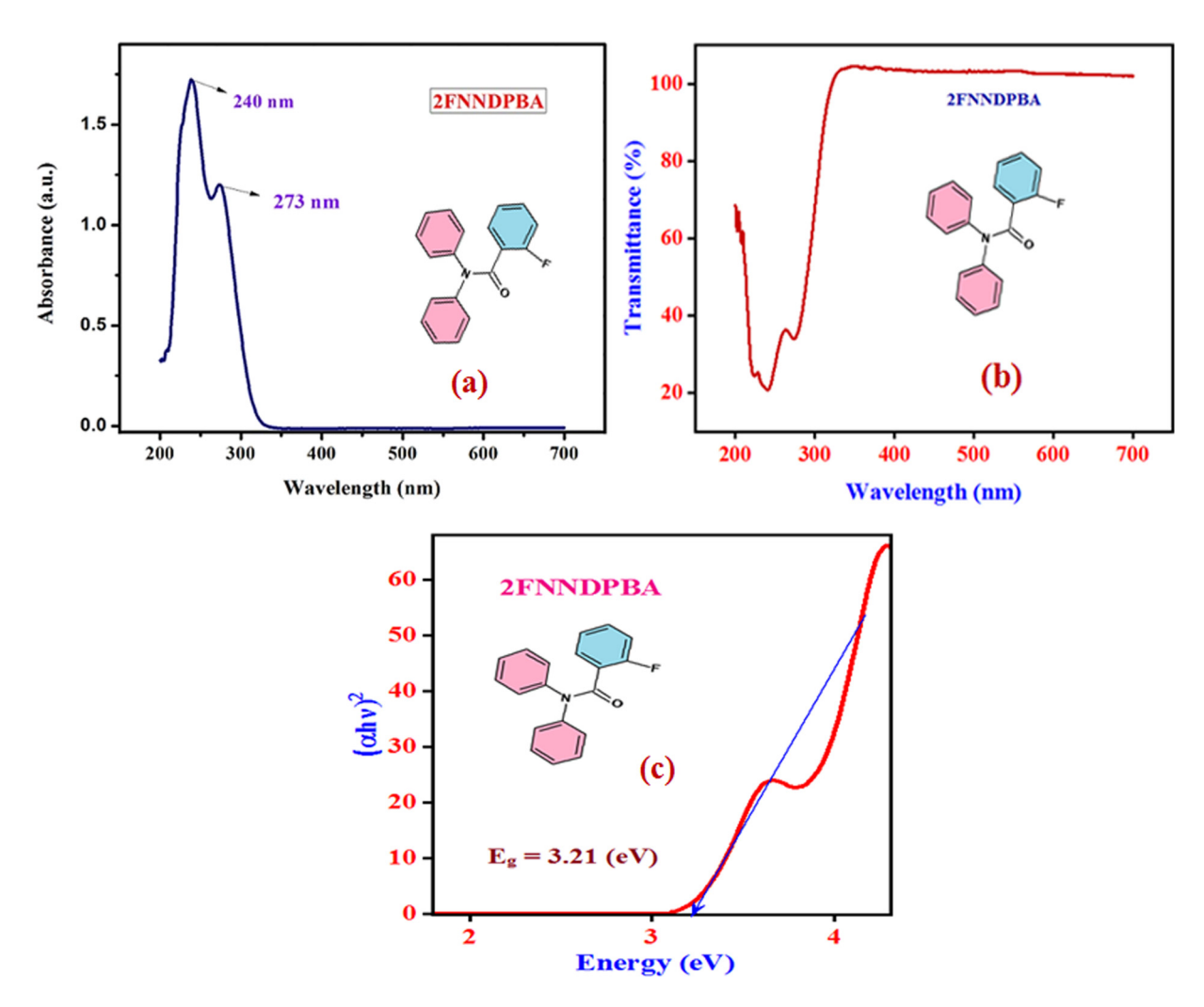


Figure 5: (a) UV-Vis-NIR absorption spectrum, (b) transmission spectrum, and (c) band gap spectra of 2FNNDPBA.

3.5 Nuclear magnetic resonance (NMR) spectral studies

NMR spectroscopy is an excellent and broadly used technique to explicate the structure of all organic compounds. In addition, the information concerning inter and intramolecular hydrogen bonding can be obtained using NMR spectroscopy. In this work, $^1\mathrm{H}$ and $^{13}\mathrm{C}$ NMR spectra of 2FNNDPBA single crystal were recorded using Burker AMX 400 FT-NMR spectrometer with the help of DMSO-d₆ as a solvent and tetramethylsilane (TMS) as a reference material. The recorded $^1\mathrm{H}$ and $^{13}\mathrm{C}$ NMR spectra of 2FNNDPBA crystal are depicted in Figure 8. The $^1\mathrm{H}$ NMR spectrum reveals that the title compound has seven types of aromatic protons. Magnetically equivalent two benzene ring protons appeared as a multiplet at $\delta=7.3$ ppm. Fluorine substituted benzene ring proton resonance occurred at $\delta=7.05$, 7.12, and 7.52 ppm.

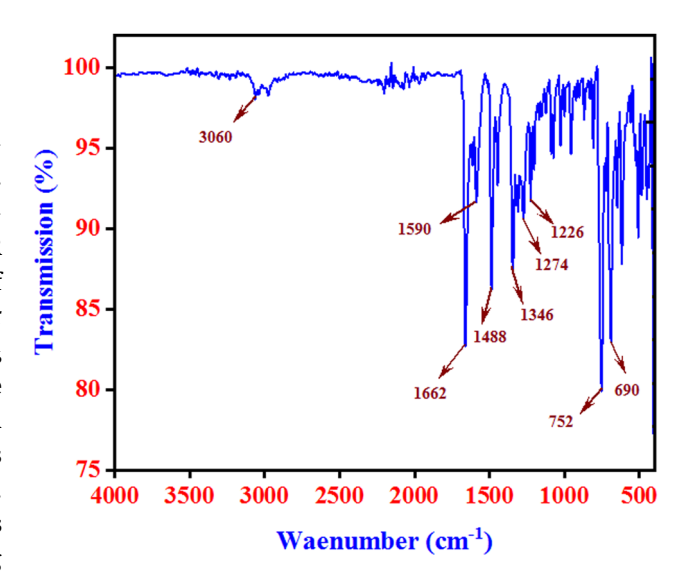


Figure 6: FT-Raman spectra of 2FNNDPBA.

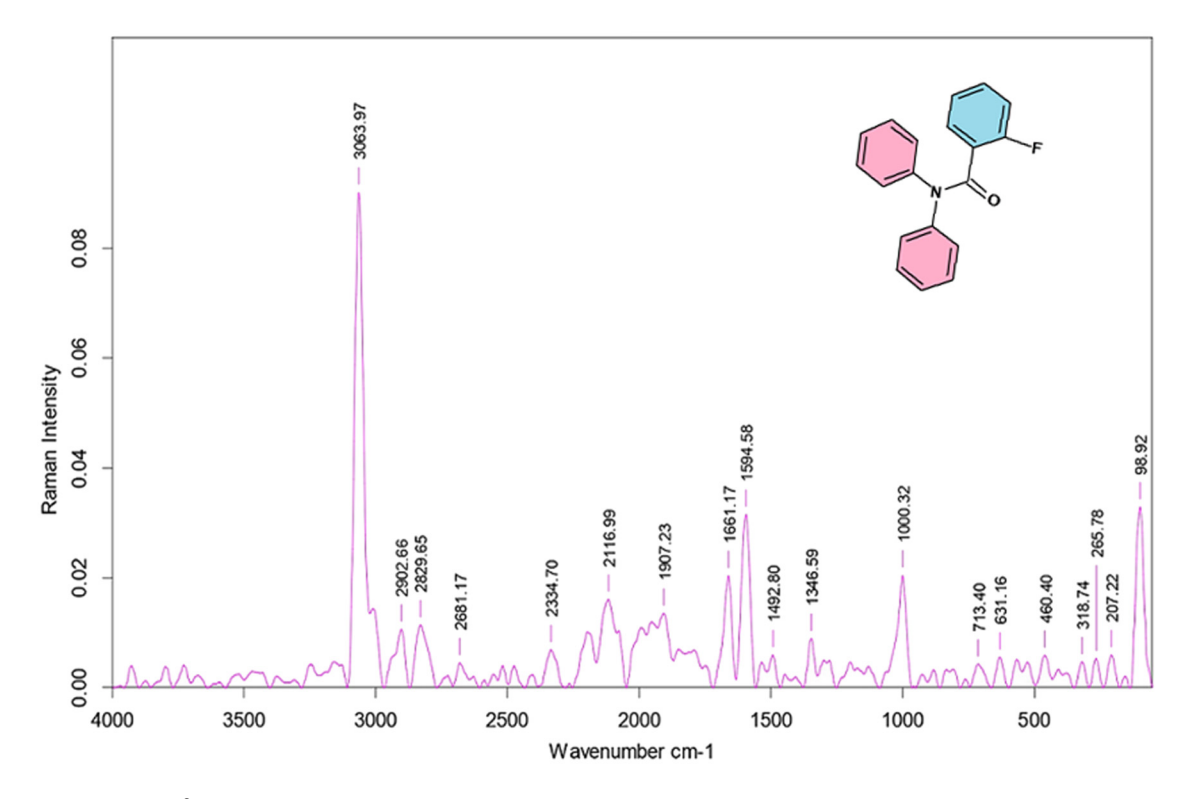


Figure 7: FT-IR spectra of 2FNNDPBA.

Table 4: FT-IR and Raman spectral data of 2FNNDPBA

FT-IR (cm ⁻¹)	FT-Raman (cm ⁻¹)	Mode of assignments
3,060	3,064	v(C-H) asymmetric vibration (aromatic)
1,662	1,661	v(C=0) stretching vibration (tertiary amide)
1,590, 1,488	1,594, 1,492	v(C=C) stretching vibration
1,346	1,347	v(C-N) asymmetric and symmetric vibrations
1,010	1,000	v(C-F) stretching vibrations
752	713	v(C=C) bending stretching vibrations

In 13 C NMR spectrum, the signal for the carbonyl carbon in the benzamide functional group, present in 2FNNDPBA moiety, appears at $\delta=167$ ppm. The signal at $\delta=159$ ppm was assigned to highly deshielded fluorine substituted aromatic carbon atom in the 2FNNDPBA compound. The remaining aromatic carbons' resonance appeared at $\delta=157$, 143, 131, 130, 128, 127, and 116 ppm, respectively.

3.6 Thermal analysis

Thermogram is used in order to get information about decomposition patterns of synthesized material and weight loss. The thermal permanence of 2FNNDPBA crystal was deliberate by thermogravimetric analysis (TGA) and differential thermal analysis (DTA) using SDT Q600 V20.9 Build 2.0 device among the temperatures 40–400°C at a heating rate of 20°C·min⁻¹ under nitrogen gas atmosphere in 100 mL·min⁻¹ purge. The resultant thermogram is shown in Figure 9. The mass of the powdered material was estimated to be 2.078 mg, with a final mass of 4.95% left over after the conduct experiment, indicating that there is no weight defeat which indicates up to 160°C. Hence, there is no evidence for any physically absorbed water in the crystal lattice or on the crystal surface. Major weight losses were observed in between 160°C and 275°C for the designated compound. The DTA curve proves that two sharp endothermic peaks at 171°C and 282°C. Thus, the crystal should have good degree of crystallinity and wholesomeness of the grown crystal.

1156 — C. Raveendiran et al. DE GRUYTER

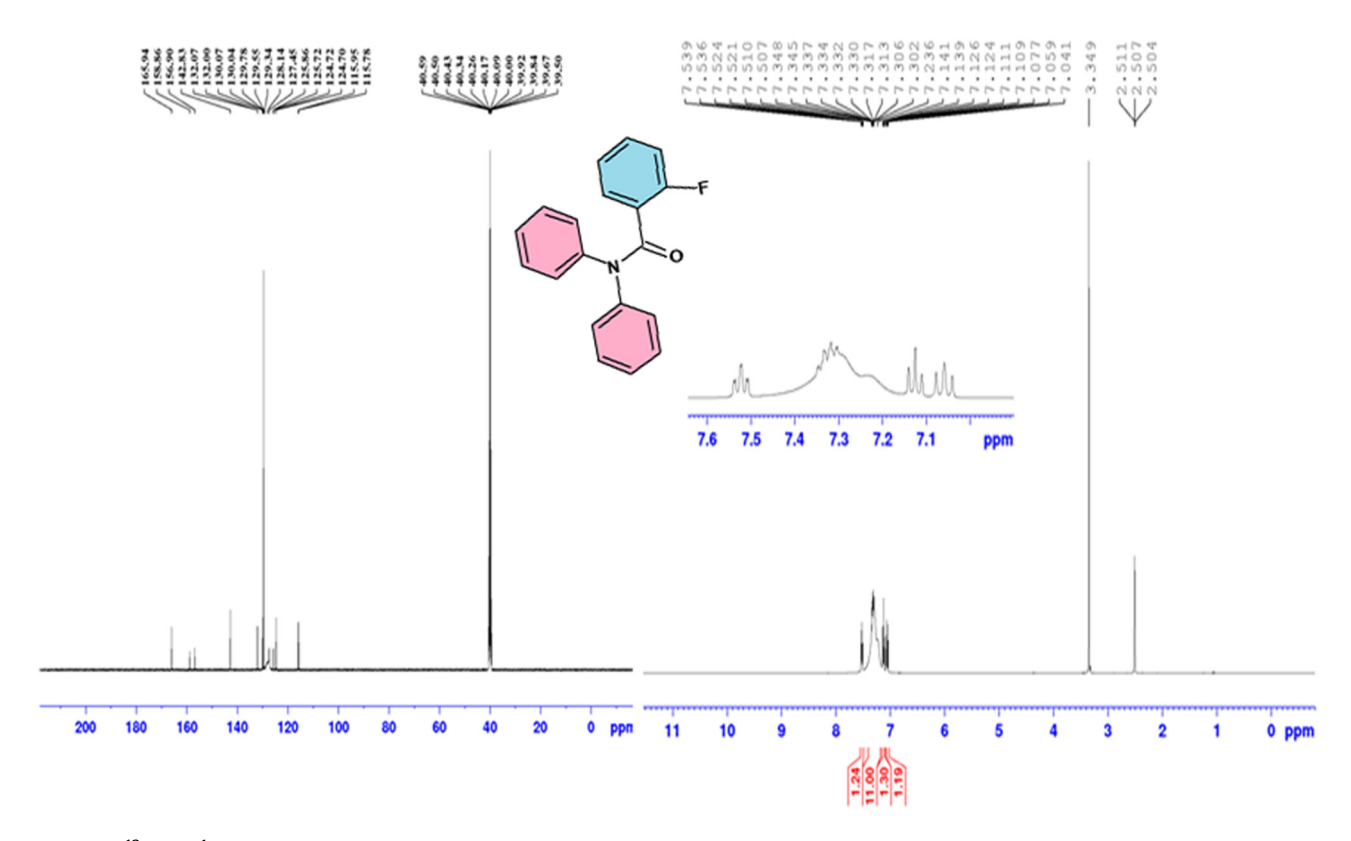


Figure 8: ¹³C and ¹H NMR spectral data of 2FNNDPBA.

3.7 Second harmonic generation efficiency

Potassium dihydrogen phosphate (KDP) crystal was used as situation material for investigating the second harmonic generation efficiency of the grown crystal 2FNNDPBA and it was assessed by the Kurtz-Perry powder technique. The powdered crystal sample is firmly packed in a microcapillary tube mounted in the course of the Q-switched Nd:YAG laser was used as a light source. The fundamental laser beam of 1,064 nm wavelength was used and input energy of 1.2 mJ per pulse was prepared to fall usually on the sample cell. The detector acts as a photomultiplier tube and the green light emitted by the sample is recorded in oscilloscope assembly. The SHG signal wavelength of 532 nm and the output energy of 122 mV were obtained for the crystal sample 2FNNDPBA, respectively. The reference material KDP displays 55 mV of similar frequency section. The second harmonic efficiency of the crystal is established to be 2.22 times of the standard KDP crystal. Better laser damage threshold of 1.18 GW·cm⁻² was observed from the sample 2FNNDPBA, when compared with standard KDP, which was 0.20 GW·cm⁻² [30,31] and the experimental values are shown in Table 5.

3.8 First-order hyperpolarizability techniques

The interaction of electromagnetic beams in a range of mediums to generate new fields modified in phase,

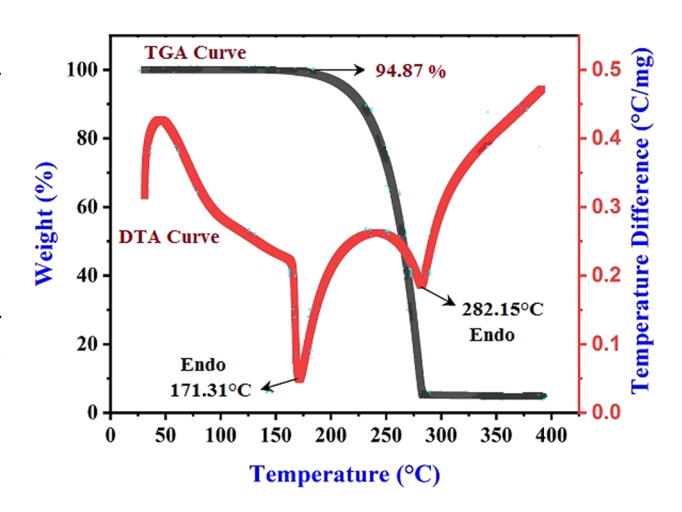


Figure 9: TGA-DTA curves of 2FNNDPBA.

amplitude, frequency, or other balanced features from the incident fields is known as NLOs [32]. The importance of frequency shifting, optical intonation, optical switching, optical logic, and optical recollection for the latest technologies in areas such as telecommunications, signal dispensation, and optical interconnections has propelled NLO to the forefront of current research [33–36].

The total dipole moment μ_{tot} of the synthesized molecule in an electric field $E_{\text{i}}(\omega)$ can be acquired by Taylor expansion as follows:

$$\mu_{\text{tot}} = \mu_0 + \alpha_{ij}E_j + \beta_{iik}E_jE_k + \dots$$
 (1)

where α is the linear polarizability, μ_0 is the permanent dipole moment, and β_{ijk} are the first hyper polarizability tensor elements. The mean (anisotropic) linear polarizability is characterized as follows [37]:

$$\alpha_{\text{tot}} = \frac{\alpha_{xx} + \alpha_{yy} + \alpha_{zz}}{3}$$
 (2)

Total polarizability is as follows:

$$\Delta \alpha = 2^{-1/2} (\alpha_{xx} - \alpha_{yy})^2 + (\alpha_{yy} - \alpha_{zz})^2 + (\alpha_{zz} - \alpha_{xx})^2 + (6\alpha_{xx}^2)^{1/2}$$
(3)

A third rank tensor of first-order hyperpolarizability is described by $3 \times 3 \times 3$ matrix. The 3D matrix of 27 elements can be reduced to 10 elements owing to Kleinman symmetry. ($\beta_{xyy} = \beta_{yxy} = \beta_{yyx} = \beta_{yyz} = \beta_{yzy} = \beta_{zyy} = \beta_{zyy} \dots$, likewise other permutations also take same value). The output from Gaussian 09W provides ten elements of this matrix as β_{xxx} , β_{xyy} , β_{xxy} , β_{xyy} , β_{yyy} , β_{yyy} , β_{xxz} , β_{xyz} , β_{xzz} , β_{yzz} , β_{zzz} , respectively. The elements of the first-order hyperpolarizability can be evaluated by the following equation [35]:

$$\beta_i = \beta_{iii} + \frac{1}{3} \sum_{i \neq i} (\beta_{ijk} + \beta_{jij} + \beta \alpha_{jji})$$
 (4)

Using the x, y, and z elements of β , the magnitude of the first hyper polarizability tensor can be estimated as follows:

$$\beta_{\text{tot}} = (\beta_x^2 + \beta_y^2 + \beta_z^2)^{1/2}$$
 (5)

where

$$\beta_{x} = (\beta_{xxx} + \beta_{xyy} + \beta_{xzz}) \tag{6}$$

$$\beta_{y} = (\beta_{yyy} + \beta_{yzz} + \beta_{xxy}) \tag{7}$$

$$\beta_{z} = (\beta_{zzz} + \beta_{yyz} + \beta_{yyz}) \tag{8}$$

The output from Gaussian 09W, the whole equation for scheming the extent of β_{tot} is given as follows:

$$\beta_{\text{tot}} = [(\beta_{xxx} + \beta_{xyy} + \beta_{xzz})^2 + (\beta_{yyy} + \beta_{yzz} + \beta_{xxy})^2 + (\beta_{zzz} + \beta_{xxz} + \beta_{yyz})^2]^{1/2}$$
(9)

The computations from the Gaussian O9W output of total molecular dipole moment (μ), linear polarizability (α), and first-order hyperpolarizability (β) have been presented in detail previously [38], and DFT has been widely employed as a competent tool to analyze organic NLO materials [39–43].

Table 6 shows the calculated hyperpolarizability values of 2FNNDPBA. The dipole moment and mean polarizability μ_{tot} in 2FNNDPBA were found to be 3.7435D and 3.9320×10^{-23} esu, in that order, with the greatest value of dipole moment in the direction μ_v equal to 1.672D. Total computed value for first-order hyperpolarizability is found to be 11.243×10^{-31} esu (Table 6). The theoretically estimated (DFT) values were transformed into electrostatic units because the values of initial hyper polarizability tensors of Gaussian 09W output are presented in atomic units (a.u.) (for α : 1 a.u. = 0.1482 × 10⁻²⁴ esu; for β : 1 a.u. = 8.6393 × 10⁻³³ esu). KDP is an excellent chemical for studying a molecule's NLO characteristics. KDP is widely employed as a threshold value for relative purposes because it is one of the prototype molecules used in the research of the NLO molecular system attributes. The first-order hyperpolarizability of KDP was found to be (KDP = 6.85×10^{-31} esu). Therefore, the first-order hyperpolarizability of the designated compound originating at virtually 1.64 times and observed to be experimentally 2.2 times that of the KDP. It can be seen that 2FNNDPBA is a polar molecule with non-zero dipole moment and polarizability values, which give the microscopic origin of this organic material's NLO activity.

3.9 Mulliken atomic charges

The Mulliken atomic charges are derived using the basis function [44] to determine the electron occupants of each

Table 5: NLO property and laser damage threshold data of 2FNNDPBA

Sample code	Output energy (mV)	Input energy (mJ·pulse ⁻¹)	Laser damage threshold (GW·cm ⁻²)
KDP	55	1.2	0.2
2FNNDPBA	122	1.2	1.18

1158 — C. Raveendiran et al. DE GRUYTER

Table 6: The electric dipole moment (μ) , polarizability $(\Delta \alpha)$, and first-order hyperpolarizability (β) of 2FNNDPBA by B3LYP/6-311++G(d,p) method

Parameters	Value	Parameters	Value	Parameters	Value
βxxx	-0.1934	α_{xx}	381.447	μ_{x}	-3.34
βχχ	-0.4523	a_{xv}	6.162	μ_{y}	1.672
βχγ	0.4727	α_{vv}	282.457	μ_{z}	0.2509
βγγγ	-0.3384	α_{xz}	11.477	μ (Debye)	3.7435
βzxx	-0.3242	a_{vz}	-2.709		
βχγχ	0.3057	α_{zz}	132.042		
βzyy	0.3553	$lpha_0$	265.3153		
βxzz	0.6223	α	3.9320×10^{-23}		
βyzz	-0.1257	Δα (a.u.)	695.5708		
βzzz	-0.2336	Δα (esu)	1.0308×10^{-22}		
β_{tot} (esu) = 11.243	× 10 ⁻³¹	. ,			

atom. Table 7 shows the Mulliken atomic charges of 2FNNDPBA molecule determined by B3LYP using the basis set 6-311++G(d,p). In the application of quantum chemical calculations of the molecular system, Mulliken atomic charge calculation is crucial. The presence of substantially electronegative oxygen and fluorine atoms (01 = -0.176271e and F36 = -0.118615e) in the neighboring position causes the maximum positive charge (1.0875e) for carbonyl group bonded phenyl C6 atom than other atoms in 2FNNDPBA. In 2FNNDPBA, the carbon atoms coupled with hydrogen atoms have a negative charge, whereas the other carbon atoms have a positive charge. All hydrogen atoms have +ve charges, whereas the nitrogen atom has a +ve charge and the oxygen atom has a -ve charge. The carbon atoms C6, C9, and C12 acquire more +ve charges, because of the flat structure, this is the case of the crystalline substance and electron-withdrawing groups bonded in the benzene ring. The continuation of a large -ve charge on C4, C5, C11, and C18 and net +ve charge on H33, H26, and H24 atoms may authorize the production of F36....H33, C5-O1....H26 and C9-H24...O1 intramolecular interaction in crystalline solid.

3.10 HOMO-LUMO analysis

The HOMO and LUMO molecular orbitals are the frontier molecular orbitals. A HOMO with electron density localized on the donor unit and a LUMO with electron density concentrated on the receiver unit are typically revealed by DFT simulations. These orbitals play a crucial function in the electrical and optical properties of the molecule, in addition the way it interacts with other species [45]. The ionization potential is represented by the HOMO energy, while the electron affinity is represented by the

LUMO energy. The energy break between HOMO and LUMO has been used to explain the stability of structures, and this gap has been used to characterize certain important concerns such as kinetic permanence and chemical reactivity of the molecule [46]. Low kinetic permanence and high chemical reactivity are more likely in compounds with a small border orbital space [36]. One of the important characteristics of the energy break between HOMO and LUMO dictated the molecule electrical transport capabilities [47–49]. The HOMO energy, LUMO energy, and energy break of 2FNNDPBA are computed using the B3LYP level with the 6-311++G(d,p) basis set, as shown in Figure 10. The molecular orbitals and energies for the HOMO–LUMO,

Table 7: Mulliken atomic charges of 2FNNDPBA by B3LYP/6-311++G(d,p) method

Atoms	Atomic charges	Atoms	Atomic charges
01	-0.176271	C19	-0.127990
N2	0.731787	C20	-0.340725
C3	-0.159669	C21	-0.264798
C4	-0.596782	H22	0.172945
C5	-0.617772	H23	0.158468
C6	1.087527	H24	0.194863
C7	0.123645	H25	0.179170
C8	0.052030	H26	0.211057
C9	0.179796	H27	0.182610
C10	0.059200	H28	0.189900
C11	-0.914547	H29	0.186528
C12	0.252776	H30	0.187211
C13	-0.219777	H31	0.152835
C14	-0.309487	H32	0.158836
C15	-0.151749	H33	0.203187
C16	-0.275461	H34	0.180608
C17	-0.387338	H35	0.174390
C18	-0.358388	F36	-0.118615

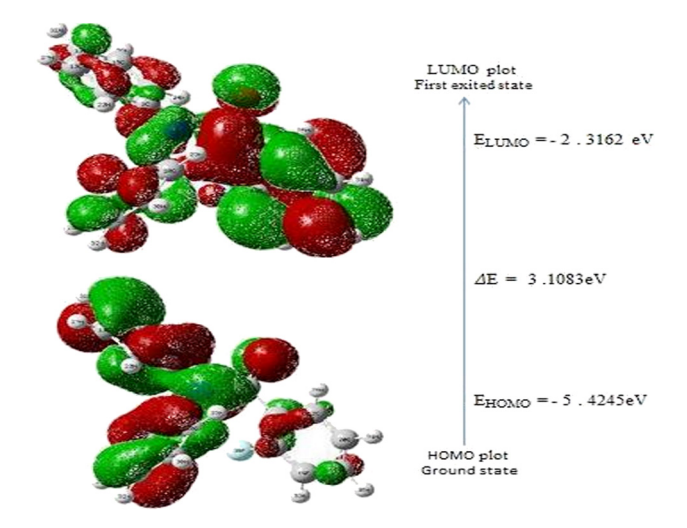


Figure 10: The molecular orbitals and energy levels for the HOMO-LUMO of 2FNNDPBA.

+ve phase, and –ve phase of the orbitals are depicted in red and green color, respectively. The rings have the highest occupied molecular orbitals and the lowest vacant molecular orbitals, indicating that the HOMO–LUMO is primarily π-antibonding. 2FNNDPBA molecule has more occupied molecular orbitals, according to the findings. The HOMO levels are predominantly diffused across *N,N*-diphenylamine, and somewhat extended on the carbonyl group present in the phenyl ring, as seen in Figure 10. LUMO levels are primarily found in 2-fluorophenyl and carbonyl groups, with the (O=C-NH-) amide moiety being partially stretched. The energy gap implies an electron density transfer from the N, N-diphenylamine benzene ring to the 2-fluorophenyl ring, as well as the ultimate charge transfer inside the molecule. The energy of LUMO is

 $-2.3162\,\mathrm{eV}$, while the energy of HOMO is $-5.4245\,\mathrm{eV}$. The frontier orbital energy gap of 2FNNDPBA is $3.1083\,\mathrm{eV}$, according to DFT calculations. Using Tauc's plots $(\alpha h v)^2$ with energy (eV), the experimental optical band gap (E_g) of the 2FNNDPBA crystal was calculated and found to be $3.21\,\mathrm{eV}$. As a result, the energy gap of the designated compound 2FNNDPBA is rather small. The ultimate charge transfer that occurs inside the molecule, which determines its high polarizability and chemical activity, is explained by the HOMO–LUMO energy gap being smaller.

3.11 MEP

The electronic density and valuable description in accepting sites for nucleophilic reaction and electrophilic assault, in addition to hydrogen bonding interactions, are both addressed by MEP [50]. MEP is also visually aware of the molecule's relative polarity. An electron density isosurface mapped with electropotential surface represents the molecule's shape, size, charge density, and reactive sites. Using Eq. 10 [51], the molecule electrostatic potential V(r) values were computed as follows:

$$V(r) = \sum_{A} Z_{A}/|R_{A} - r| - \int \rho(r^{1})/|r^{1} - r|d^{3}r^{1}$$
 (10)

where Z_A is the charge of nucleus A at R_A , $\rho(r^1)$ is the electronic density function, and r^1 is the model integration variable. The electrostatic potential has different values at the surface and is represented by different colors: most –ve electrostatic potential regions are represented by red, most +ve electrostatic potential regions are

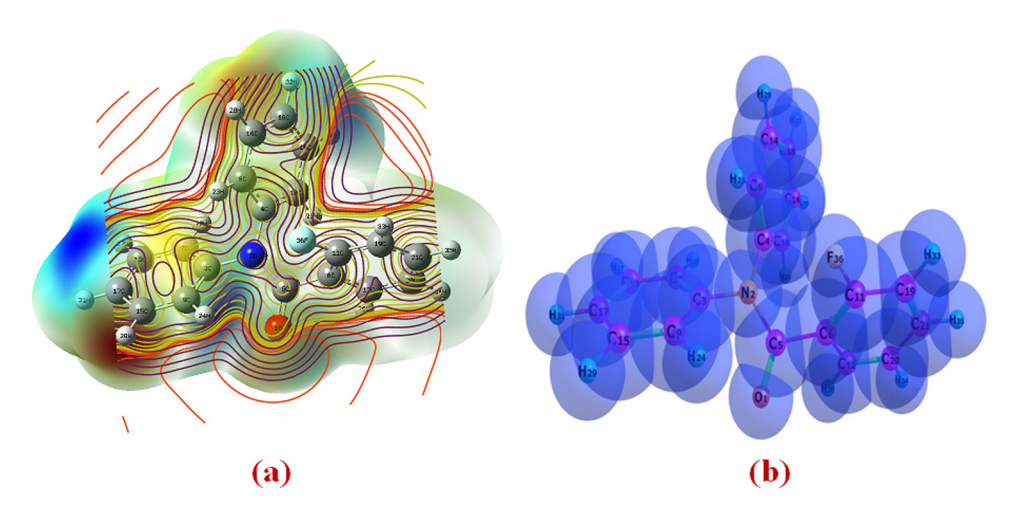


Figure 11: (a) Molecular electrostatic potential map calculated at B3LYP/6-311++G(d,p) level. (b) Van der Waals radii calculated at B3LYP/6-311++G(d,p) level.

represented by blue, and close to zero potential regions are represented by green. The electrostatic potential increases in the order of red < orange < yellow < green < blue [52].

The electrostatic surface potential at the B3LYP/6-311++G(d,p) optimized geometry is used to compute reactive sites for nucleophilic and electrophilic processes for the considered molecule. As seen in Figure 11, the discovered molecule has a variety of possible electrophilic and nucleophilic attack sites. The electrostatic potential variations are from -0.0076 to +0.0076 a.u., with deep blue density indicating extremely electron deficient areas (V(r) > 0.0076 a.u.) and mild red indicating extremely electron abundant areas (V(r) < -0.0076 a.u.). According to Figure 11a, the maximum –ve area on the oxygen atom of the O1 in carbonyl amide group is -0.0076 a.u. and -0.0076 a.u., respectively, while the maximum +ve area localized on the C3-N2 and C13-N2 bond is +0.0076 a.u. and +0.0076 a.u., respectively, representing a possible site for electrophilic attack and nucleophilic reaction. The resulting MEP map shows +ve potential sites surrounding hydrogen atoms and -ve potential sites on electronegative oxygen atoms, based on the estimated values. The information of inter- and intra-molecular connections and van der Waals radii is provided by Figure 11a and b.

4 Conclusion

Optically worth single crystals of 2FNNDPBA were grown by the slow evaporation solution growth technique. The XRD study of the single-crystal reveals that the 2FNNDPBA grown single crystals belong to the orthorhombic system with centrosymmetric space group *Pbca*. The vibrational stretching frequencies and NMR studies identify the functional groups in the grown crystal. The crystal has a reduced cut-off wavelength of 240 nm, indicating that 2FNNDPBA could be used to make a near-ultraviolet NLO crystal. The electronic bandgap and electric receptiveness were found to be experimentally 3.21 eV and theoretically 3.1083 eV, respectively. The DTA curve proves the presence of two sharp endothermic peaks at 171°C and 282°C. TG-DTA thermal studies confirm that the grown single crystals are thermally secure up to 171°C. The NLO test accentuates that 2FNNDPBA makes obvious SHG efficiency of 2.22 times that of KDP and the calculated first-order hyperpolarizability was found to be 1.64 times greater than that of standard NLO material. The obtained Mulliken atomic charges of the 2FNNDPBA suggest that the oxygen atom is negative and all hydrogen atoms are positive, hence, charge transfer takes place from oxygen to hydrogen. The little HOMO-LUMO energy gap value has a widespread influence on the intramolecular charge transfer of the molecules. As a result of all these criteria, the 2FNNDPBA crystals might be a potential and a competitive contestant for future photonic devices.

Acknowledgement: The authors are thankful to SAIF, IIT Madras, India to avail single crystal X-ray diffractometer facility.

Funding information: The project was supported by Researchers Supporting Project number (RSP2023R143). King Saud University, Riyadh, Saudi Arabia.

Author contributions: C. Raveendiran, P. Prabukanthan, and J. Madhavan: conceptualization, investigation, supervision, formal analysis, methodology, validation, writing original draft, and visualization; P.A. Vivekanand: methodology, validation, and writing - review and editing; Natarajan Arumugam, Abdulrahman I. Almansour, Raju Suresh Kumar, and Karthikeyan Perumal: project administration, visualization, and writing - review and editing. Shatha Ibrahim Alaqeel: writing - review and editing and acquisition of the financial support for the project.

Conflict of interest: Authors state no conflict of interest.

Data availability statement: All materials for this study are presented in this article and available on request to the corresponding author.

References

- Evans OR, Lin W. Crystal engineering of NLO materials based [1] on metal-organic coordination networks. Acc Chem Res. 2002;35:511-22. doi: 10.1021/ar0001012.
- Zyss J, Nicoud JF, Coquillay M. Chirality and hydrogen bonding in molecular crystals for phase-matched second-harmonic generation: N-(4-nitrophenyl)-(L)-prolinol (NPP). J Chem Phys. 1984;81:4160-7. doi: 10.1063/1.448134.
- [3] Prabukanthana P, Lakshmia R, Harichandran G, Sudarsana Kumar C. Synthesis, structural, optical and thermal properties of N-methyl N-aryl benzamide organic single crystals grown by a slow evaporation technique. J Mol Struct. 2018;1156:62-73. doi: 10.1016/j.molstruc.2017.11.075.
- [4] Reshak AH, Stys D, Auluck S, Kityk IV. Dispersion of linear and nonlinear optical susceptibilities and the hyperpolarizability of 3-methyl-4-phenyl-5-(2-pyridyl)-1,2,4-triazole. Phys Chem Chem Phys. 2011;13:2945-52. doi: 10.1039/c0cp01601b.
- Latha N, Barathi D, Uthaya Kumar M, Vennila KN, Vinitha G, Mani R, et al. Structural, theoretical and third order nonlinear optical properties of (E)-N'-(4-chlorobenzylidene)-4-

- fluorobenzohydrazide monohydrate. Mol Cryst Lig Cryst. 2021:725:66-80.
- [6] Toy M, Vural H, Şenöz H. Synthesis, spectroscopic (FT-IR, ¹H NMR, and UV-Vis) and nonlinear optical properties of a novel 3-(p-Cyanophenyl)-5-(o, m, p-lodophenyl)-1-phenylformazan: experimental and DFT studies. Polycycl Aromat Compd. 2022;1-18. doi: 10.1080/10406638.2022.2133903.
- [7] Wen J, Ping L, Li R, Shang S, Zhao W, Hai M, et al. Synthesis and characterization of new benzo[e]indol salts for secondorder nonlinear optics. Crystals. 2020;10(4):242. doi: 10.3390/cryst10040242.
- Hu Z-Q, Xu D-J, Xu Y-Z. (S)-Alanine-(S)-mandelic acid (1/1). Acta Cryst. 2004;60:0269-71. doi: 10.1107/ s160053680400145x.
- Sankar K, Rajasekaran R, Vetrivelan V. Synthesis, growth and characterization of glycine ammonium bromide: a potential NLO material. Mater Today Proc. 2019;8:332-6. doi: 10.1016/ i.matpr.2019.02.119.
- [10] Parr RG, Yang W. Density functional theory of atoms and molecules. New York, Oxford: Oxford University Press; 1989.
- [11] Krishnakumar V, Balachandran V. Structures and vibrational frequencies of 2-hydroxy-3-methoxy-5-nitrobenzaldehyde and 2-methoxy-1-naphthaldehyde based on density functional theory calculations. Spectrochim Acta Part A. 2006;63:464-76. doi: 10.1016/j.saa.2005.05.032.
- [12] Altun A, Golcuk K, Kumru M. Theoretical and experimental studies of the vibrational spectra of m-methylaniline. J Mol Struct. 2003;625(1-3):17-24. doi: 10.1016/s0166-1280 (02) 00698-x.
- [13] Tabrizi MZ, Tayyari SF, Tayyari F, Behforouz M. Fourier transform infrared and Raman spectra, vibrational assignment and density functional theory calculations of naphthazarin spectrochim. Acta A. 2004;60:111-20. doi: 10.1016/s1386-1425(03) 00186-0.
- [14] Lee C, Yang W, Parr RG. Development of the Colle-Salvetti correlation-energy formula into a functional of the electron density. Phys Rev B. 1988;37:785-9. doi: 10.1103/physrevb.
- [15] Vetrivelan V. Spectra, electronic structure, biological activities and molecular docking investigation on methyl (2E)-2-{[N-(2formylphenyl)-4-methyl benzene sulfonamido] methyl}-3-(naphthalen-1-yl) prop-2-enoate: an experimental and computational approach. Mater Today Proc. 2019;8:402-11. doi: 10.1016/j.matpr.2019.02.129.
- [16] Karabacak M, Kurt M, Atac A. Experimental and theoretical FT-IR and FT-Raman spectroscopic analysis of N1-methyl-2chloroaniline. J Phys Org Chem. 2009;22:321-30. doi: 10.1002/poc.1480.
- [17] Jovita JV, Boopathi K, Ramasamy P, Ramanand A, Sagayaraj P. Synthesis, growth and characterization of 4-methyl aniliniumphenolsulfonate single crystal. J Cryst Growth. 2013;380:218-23. doi: 10.1016/j.jcrysgro.2013.06.027.
- [18] Ditchfield R, Hehra WJ, Pople JA. Self-consistent molecularorbital methods. IX. An extended Gaussian-type basis for molecular-orbital studies of organic molecules. J Chem Phys. 1971;54:724-8. doi: 10.1063/1.1674902.
- [19] Dennington R, Keith T, Millam J. Gauss view, version 4.1.2. Shawnee mission, KS: Semichem Inc.; 2007.
- [20] Frisch MJ. Gaussian 09. Wallingford, CT, USA: Gaussian Inc; 2009.

- [21] Gulluoglu MT, Erdogu Y, Karpagam Sundaraganesan J, Yurdakal S. DFT, FT-Raman, FT-IR and FT-NMR studies of 4-phenylimidazole. J Mol Struct. 2011;990:14-20.
- [22] Sheldrick GM. A short history of SHELX. Acta Cryst. 2008;64(1):112-22. doi: 10.1107/s0108767307043930.
- [23] Spek AL. Single-crystal structure validation with the program PLATON. J Appl Crystallogr. 2003;36:7-1313. doi: 10.1107/ s0021889802022112.
- [24] Farrugia LJ. ORTEP-3 for windows a version of ORTEP-III with a graphical user interface (GUI). J Appl Crystallogr. 1997;30:565. doi: 10.1107/s0021889897003117.
- [25] Bruno IJ, Cole JC, Edgington PR, Kessler MK, Macrae CF, McCabe P, et al. New software for searching the Cambridge structural database and visualizing crystal structures. Acta Crystallogr Sect B: Struct Sci. 2002;58:389-97. doi: 10.1107/ s0108768102003324.
- [26] Varsanyi G. Assignments of vibrational spectra of seven hundred benzene derivatives. London: Adam Hilger; 1974. p. 1-2
- [27] Vetrivelan V. Spectra, electronic properties, biological activities and molecular docking investigation on sulfonamide derivative compound: an experimental and computational approach. J Nanosci Tech. 2018;4(2):348-52. doi: 10.30799/ jnst.sp203.18040203.
- [28] Chandran A, Mary YS, Varghese HT, Panicker CY, Pazdera P, Rajendran G. FT-IR, FT-Raman spectroscopy and computational study of (E)-4-((anthracen-9-ylmethylene)amino)-N-carbamimidoylbenzene sulfonamide. Spectrochim Acta Part A Mol Biomol Spectrosc. 2011;79:1584-92. doi: 10.1016/j.saa.2011.05.015.
- [29] Kurt M, ChinnaBabu P, Sundaraganesan N, Cinar M, Karabacak M. Molecular structure, vibrational, UV and NBO analysis of 4-chloro-7-nitrobenzofurazan by DFT calculations. Spectrochim Acta Part A Mol Biomol Spectrosc. 2011;79:1162-70. doi: 10.1016/j.saa.2011.04.037.
- [30] Ajitha Sweetly M. Characterization of mixed crystals of sodium chloride and sodium bromate and the doped nickel sulphate crystals. Int J Res Eng Technol. 2014;3(5):189-98. doi: 10.15623/ijret.2014.0305038.
- Irusan T, Arivouli D, Ramasamy P. Microhardness studies on ammonium acid urate crystals. J Mater Sci Lett. 1993;12(6):405. doi: 10.1007/bf00609167.
- [32] Chakkaravarthy P, Vetrivelan V, Syed Shafi S, Muthu S. Spectroscopic (FT-IR & FT-Raman), Fukui function and molecular docking analysis of 6-amino-7,9-dihydropurine-8-thione by DFT approach. Bulg Chem Commun. 2020;52(4):440-4. doi: 10.34049/bcc.52.4.5234.
- [33] Andraud C, Brotin T, Garcia C, Pelle F, Goldner P, Bigot B, et al. Theoretical and experimental investigations of the nonlinear optical properties of vanillin, polyenovanillin, and bisvanillin derivatives. J Am Chem Soc. 1994;116:2094-102. doi: 10.1021/ ja00084a055.
- Geskin VM, Lambert C, Bredas JL. Origin of high second- and [34] third-order nonlinear optical response in ammonio/borato diphenylpolyene zwitterions: the remarkable role of polarized aromatic groups. J Am Chem Soc. 2003;125:15651-8. doi: 10.1021/ja035862p.
- [35] Nalano M, Fujita H, Takahata M, Yamaguchi K. Theoretical study on second hyperpolarizabilities of phenylacetylene dendrimer: toward an understanding of structure-property relation in NLO responses of fractal antenna dendrimers. J Am Chem Soc. 2002;124:9648-55. doi: 10.1021/ja0115969.

- [36] Sajan D, Joe IH, Jayakumar VS, Zaleski J. Structural and electronic contributions to hyperpolarizability in methyl p-hydroxy benzoate. J Mol Struct. 2006;785:43-5. doi: 10.1016/ j.molstruc.2005.09.041.
- [37] Socrates G. Infrared characteristic group frequencies. New York, USA: Wiley Interscience Publication; 1980.
- [38] Thanthiriwatte KS, de silva Nalin KM. Non-linear optical properties of novel fluorenyl derivatives—ab initio quantum chemical calculations. J Mol Struct Theochem. 2002;617:169-75. doi: 10.1016/s0166-1280(02)00419-0.
- [39] Sun YX, Hao QI, Yu ZX, Wei WX, Lu LD, Wang X. Experimental and density functional studies on 4-(4-cyanobenzylideneamino)antipyrine. Mol Phys. 2009;107:223-35. doi: 10.1080/ 00268970902769471.
- [40] Ahmed AB, Feki H, Abid Y, Boughzala H, Minot C, Malayah A. Crystal structure, vibrational spectra and theoretical studies of l-histidinium dihydrogen phosphate-phosphoric acid. J Mol Struct. 2009;920:1-7. doi: 10.1016/j.molstruc.2008.09.029.
- [41] Abraham JP, Sajan D, Shttigar V, Dharma Prakash SM, Nemec I, Joe IH, et al. Efficient π-electron conjugated push-pull nonlinear optical chromophore 1-(4-methoxyphenyl)-3-(3,4dimethoxyphenyl)-2-propen-1-one: A vibrational spectral study. J Mol Struct. 2009;917:27-36. doi: 10.1016/j.molstruc. 2008.06.031.
- [42] Sadine SG, Esme A. Theoretical and vibrational studies of 4,5diphenyl-2-2 oxazole propionic acid (oxaprozin). Spectrochim Acta A. 2010;75:1370-6. doi: 10.1016/j.saa.2010.01.004.
- [43] Ahmed AB, Feki H, Abid Y, Boughzala H, Minot C. Crystal studies, vibrational spectra and non-linear optical properties of

- l-histidine chloride monohydrate. Spectrochim Acta A. 2010;75:293-8. doi: 10.1016/j.saa.2009.10.026.
- [44] Mulliken RS. Electronic population analysis on LCAO-MO molecular wave functions. I. J Chem Phys. 1995;23:1833-40. doi: 10.1063/1.1740588.
- [45] Fleming I. Frontier orbitals, organic chemical reactions. London: Wiley; 1976. doi: 10.1002/nadc.19770250113.
- [46] Curtiss LA, Redfern PC, Raghavachari K. J A Pople J Chem Phys. 1998;42:117-22.
- [47] Fukui K. Role of frontier orbitals in chemical reactions. Science. 1982;218:747-54. doi: 10.1126/science.218.4574.747.
- [48] Udhayakala P, Rajendiran T, Seshadri S, Gunasekaran S. Quantum chemical vibrational study, molecular property and HOMO-LUMO energies of 3-bromoacetophenone for pharmaceutical application. J Chem Pharm Res. 2011;3(3):610-25.
- [49] Subramanian N, Sundaraganesan N, Jayabharathi J. Molecular structure, spectroscopic (FT-IR, FT-Raman, NMR, UV) studies and first-order molecular hyperpolarizabilities of 1,2-bis(3methoxy-4-hydroxybenzylidene)hydrazine by density functional method. Spectrochim Acta A. 2010;76:259-69. doi: 10.1016/j.saa.2010.03.033.
- [50] Okulik N, Jubert AH. Internet electron. J Mol Des. 2005;4:17-30.
- [51] Politzer P, Murray JS. The fundamental nature and role of the electrostatic potential in atoms and molecules. Theor Chem Acc. 2002;1087:134-42. doi: 10.1007/s00214-002-0363-9.
- [52] Thul P, Gupta VP, Ram VJ, Tandon P. Structural and spectroscopic studies on 2-pyranones. Spectrochim Acta A. 2010;75:251-60. doi: 10.1016/j.saa.2009.10.020.